Climate Dynamics (2021) 56:2469–2486
https://doi.org/10.1007/s00382-021-05677-0

Poleward shift and intensified variability of Kuroshio-Oyashio extension and North Pacific Transition Zone under climate change

Gian Giacomo Navarra[1] · Emanuele Di Lorenzo[1]

Received: 24 February 2020 / Accepted: 21 December 2020 / Published online: 4 February 2021

Abstract
The climate variability of the Kuroshio-Oyashio Extension (KOE) and North Pacific Transition Zone (NPTZ) exerts a strong control on marine populations that are sensitive to the strong productivity gradients between the subtropical and subpolar recirculation gyres. In observations, the relationship between KOE, NPTZ and productivity is evident in the first two dominant covariability modes between sea surface height and Chlorophyll-a anomalies, which are associated with a meridional shift in the location of the KOE (e.g. shift mode 1) and an intensification of the mean circulation of the KOE (e.g. intensification mode 2). To understand the projected impacts of anthropogenic forcing on the NPTZ, we examine these two dominant modes of variability in the Community Earth System Model Large Ensemble (CESM-LE) and an ensemble of climate models from the Coupled Model Intercomparing Project (CMIP5-E) under the Representative Concentration Pathways (RCP8.5). A significant poleward shift has been found in the KOE mean location associated with an equivalent shift of the Aleutian Low atmospheric pressure system. Superimposed to the changes of the mean, we find a significant increase (15–20%) in the variability of the shift mode in both the CESM-LE and CMPI5-E suggesting that variation in the meridional position of the NPTZ are also becoming stronger. These changes in variance of the shift mode are linked to an increase variability of the atmospheric forcing.

Keywords North pacific transition zone · Kuroshio-oyashio extension · Western boundary current · Marine ecosystem variability · Climate change

1 Introduction

The Kuroshio-Oyashio Extension (KOE) represents the western boundary current development of the subtropical gyre. When the Kuroshio and Oyashio currents separates from the Eastern part of Japan, at 35 ° N they form the KOE, which is characterized by quasi stationary meanders formed in the Izu-Ogasawara Ridge (Qiu 2002; Qiu and Chen 2005). In this region high interactions between atmosphere and ocean take place. The oceanic features of the KOE can be described through heat transfers that are mainly latent and sensible energy fluxes. In particular the connection between winds and multi-scale ocean variability play a key role in the climate system by maintaining the surface baroclinicity and energizing storms (Kwon et al. 2010; Sasaki and Schneider. 2011).

The KOE is part of a larger region between the subpolar and subtropical gyre that is also referred to as the North Pacific Transition Zone (NPTZ) (Fig. 1a, black box). This region is characterized by the presence of a strong chlorophyll-a (CHL-a) front and is defined as the contour where CHL-a equals 0.2 mg m^{-3} (Ascani et al. 2016; Polovina et al. 2001,2015; Sasai et al. 2007). The seasonal changes of the NPTZ, it is South of the KOE in boreal winter while in Summer it moves North of the jet, make it crucial for physical and biological reasons. Ocean turtles follow the meridional seasonal migrations of the NPTZ, specifically the sharp surface chlorophyll gradient. These migrations of the front are characterized by strong interannual to decadal variability linked to the KOE dynamics and are evident as a region of high correlation between CHL-a and sea surface height anomalies (SSHa) (Fig. 1b, black box).

✉ Gian Giacomo Navarra
gnavarra3@gatech.edu

Emanuele Di Lorenzo
edl@gatech.edu

[1] Program in Ocean Science and Engineering, Georgia Institute of Technology, 311 First Drive NE, Atlanta, GA 30332, USA

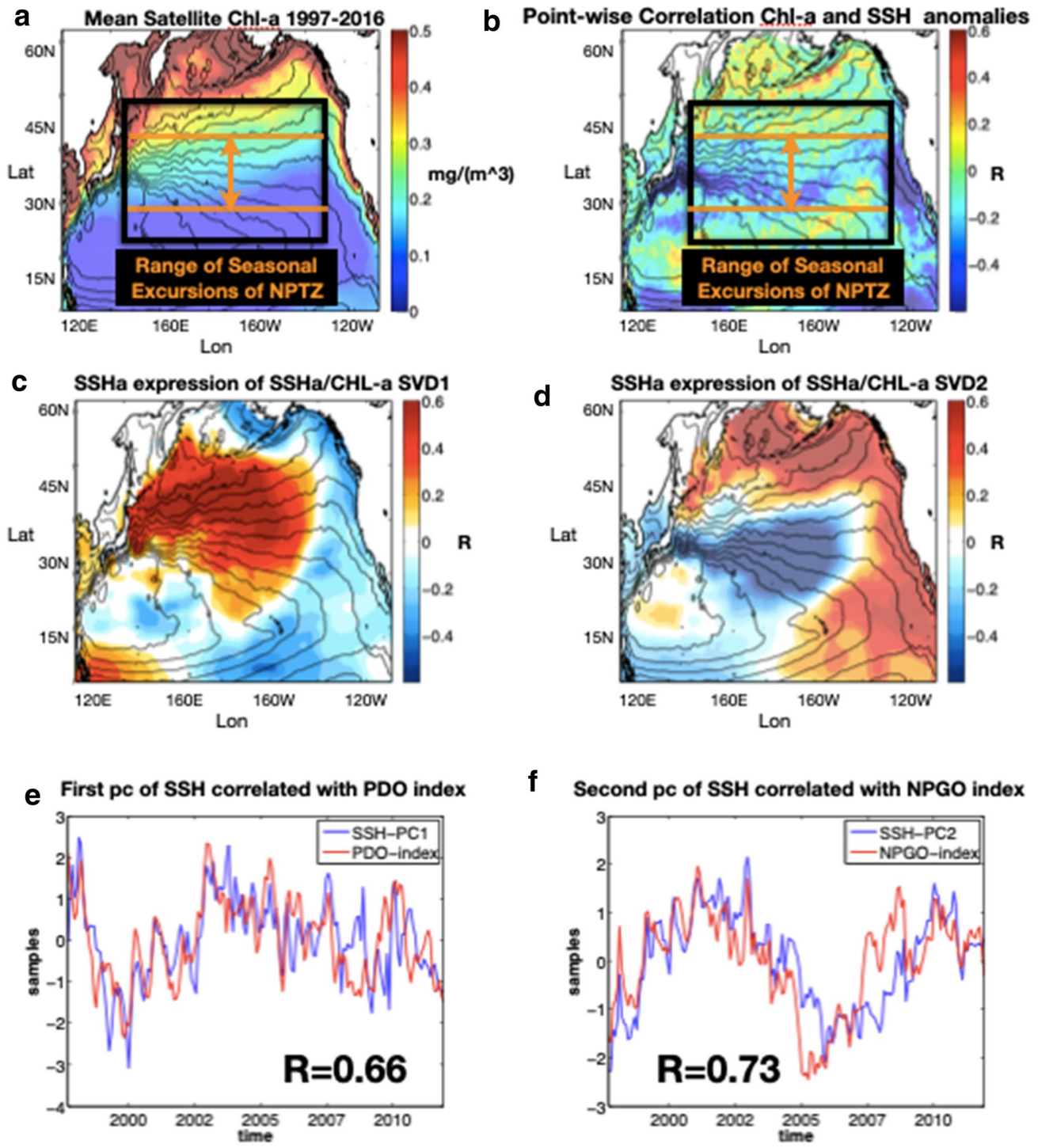

Fig. 1 In (**a**) the mean chlorophyll concentration is displayes with particular relevance to the NPTz area of loggerhead turtules seasonal migrations. **b** Displays the total correlation between SSH and the Chl-a. In (**c**) the first pattern of SSh obtained from SVD analysis between the SSH adn the chlorophyll is shown. The second pattern in (**d**). The line contours if **a**–**d** represent the mean dynamic ocean topography (MDOT) for the SSH. Then the last two figures display how the first SSH pc correlates with PDO index (**e**) and how the second SSH pc correlates with the NPGO index (**f**)

The KOE is also known to be one of the major regions of decadal variability in the North Pacific. The origins of these low-frequency fluctuations are linked to both internally generated and externally forced mechanisms. Although some studies suggest that instabilities and eddy mean flow interactions act as an important mechanism for generating internal decadal variability (Yang and San Liang 2018; Pierini and Dijkstra 2009; Taguchi et al. 2010), most studies have identified external atmospheric forcing through the excitation of large-scale ocean Rossby waves as the more dominant driver of KOE decadal variability (Qiu 2003; Qiu and Chen 2005; Ceballos et al. 2009; Yang et al. 2017). Specifically, the low-frequency variability of the KOE and NPTZ is linked to large-scale atmospheric forcing associated with the variability of the Aleutian Low (AL) (Qiu et al. 2007) and the North Pacific Oscillation (NPO) (Ceballos et al. 2009). The AL and NPO drive the oceanic variability of the PDO and of the North Pacific Gyre Oscillation (NPGO), respectively. The adjustment of the PDO and NPGO SSHa is known to excite long Rossby waves in the central and eastern North Pacific that propagate westward towards the western boundary where they energize the decadal variability of the KOE (Minobe 1999; Taguchi et al. 2005). In recent years Wu et al. (2019) argue that another candidate for the generation of westward propagating Rossby waves is the Atlantic-Multi-decadal Oscillation (AMO). The AMO wind induced anomalies propagate westward at the speed of the first mode baroclinic Rossby wave.

The impact of decadal fluctuations of the KOE on the NPTZ and marine ecosystem is well documented. It has been found that the seasonal migration of juvenile turtles is influenced by the decadal changes in the mean location of the NPTZ in connection with the KOE position and phases of the Pacific Decadal Oscillation (PDO) (Mantua et al. 2002; Ascani et al. 2016). When the PDO is in positive phase, that is a positive value of the associated index, the KOE weakens allowing the neonates to move north where they find more productive waters. On the opposite during a negative phase of the PDO the KOE strengthen and the loggerhead neonates move South in the less productive waters of the Subtropical gyre. One explanation of this relation is linked to the way the PDO interacts with primary production. When the AL intensifies (positive phase of the PDO) it leads to an increase in wind stress and the vertical mixing of cold water in the upper ocean. The resulting deepening of the mix layer leads to less availability of light in the euphotic layer and an overall reduction of zooplankton biomass (Yatsu et al. 2013; Nakata et al. 2001). The loggerheads turtles will then move north to find more productive waters in the Oyashio region.

Although vertical mixing of nutrient is clearly an important driver of ecosystem variability in the KOE, horizontal transport dynamics play an equally important role (Di Lorenzo et al. 2013a, b). From previous studies it has been confirmed the role of the AL/PDO in inducing temporal variations in the KOE zooplankton by dominating the seasonal mixed layer process (Chiba et al. 2009a, b). However, it has also been shown that changes in the NPO/NPGO modify the mean advective transport of the KOE and impact the zooplankton biogeography (Chiba et al. 2013).

Given the reliance of marine ecosystem and fisheries on the interannual and decadal variability of the NPTZ, the goal of this study is to explore how the NPTZ variance responds to a warmer climate predicted by global climate models. Specifically, we examine the Community Earth System Model Large Ensemble (CESM-LENS) projection and compare against an ensemble of climate models from the Coupled Model Intercomparing Project (CMIP5) under the Representative Concentration Pathways RCP8.5. Previous studies have already noted that western boundary currents, such as the KOE, are likely shifting poleward and intensifying as a result of climate warming (Yang et al. 2016; Lorenz 2014), however, it remains unclear if these changes in the mean are also followed by a change in the variability—which may have even more important impacts on marine populations (Sydeman et al. 2013).

The article is organized in sections as follows. The covariance analysis between SSHa and CHL-a is described in Sect. 3 and is used to identify the physical signatures of the NPTZ variability in the KOE modes. In Sect. 4 the future scenario of the SSH variance is described considering the CMIP5-E models and CESM-LE runs. In the last section the sea level pressure (SLP) pattern that guide the SSH in the Kuroshio have been taken into consideration.

The main purpose is to analyze the future scenario of the SSH variance. We also connect this change to the atmospheric influence of SLP variations on KOE and how it will change in time. The importance of considering the variance of SSH connect to his biological implications.

2 Data and methods

The SSH altimeter data is produced by the Copernicus Marine Service and it derived by merging multimission altimeter data from the following missions: Jason-3, Sentinel-3A, HY-2A, Saral/AltiKa, Cryosat-2, Jason-2, Jason-1, T/P, ENVISAT, GFO, ERS1/2. Further description and download of the data is found in https://resources.marine.copernicus.eu/?option=com_csw&task=results?option=com_csw&view=details&product_id=SEALEVEL_GLO_PHY_L4_REP_OBSERVATIONS_008_047.

For the chlorophyll we use the data from the ocean Colour CCI project which focusses on the water-leaving radiance in the visible domain. Derived chlorophyll and inherent optical properties utilize data archives from ESA's globally merged MERIS, NASA's SeaWiFS and MODIS sensors archives. It is also looking at the feasibility of using OCM-2 and VIIRS data as a "gap filter" before the launch of Sentinel-3. Further informations are found in. https://esa-oceancolour-cci.org/

The SSH dataset used in this study has a 1/4 × 1/4 spatial resolution. It covers the period from 1993 to 2017 and consists of monthly mean values. The grid goes from 50 S to 61 N of latitude and from − 260 to − 50 of longitude. The chlorophyll data have been put on the same spatial grid.

2.1 Variance trend calculation

The method used to obtain the variance can be described. After calculating the absolute value of the first principal component, a Taylor expansion $y_{tr} = x_o + x_1 t + x_2 t^2$ has been considered. In this case t is the length of the ensemble mean first pc. We have then two vectors, one of the coefficients $x = [x_o\ x_1\ x_2\ \ldots]$ and the other of the variable $E = [1\ t\ t^2 \ldots]$. If we define $y_{tr} = Ex$, the variance is obtained by minimizing the square minly-$Ex|^2 = 0$

$$J = n^T n = (y - Ex)^T (y - Ex)$$
$$\frac{\partial J}{\partial x} = -2E^T (y - Ex) = 0 \qquad (1)$$
$$x = \left(E^T E\right)^{-1} E^T y$$

y is the first principle component. The same procedure has been done for the second pc. This is a kind of linear regression, with a numerical error that depends on when the series is stopped.

2.2 Model output

The data sets used in the model part are two kind of series, a CMIP5-E/historical and a CMIP5-E/RCP8.5. This kind of model is a coupled ocean–atmosphere model where the atmosphere is represented as a stochastic interference in the ocean. For the analyses 23 different types of CMIP5-E models are considered. The reasons why there is not only one model of coupled atmosphere–ocean depends on the fact that the stochastic interference can be treated in many different ways. The list of those models is present in Table 1.

The models extend from 90 S to 90 N, with 1 degree of resolution. The data for SSH and SLP can be found in http://apdrc.soest.hawaii.edu/dods/public_data/CMIP5. Then the results from these models have been compared with the output of the CESM model alone in order to verify the results.

2.3 CESM-LE model runs

We compare the results of the CMIP5-E with 29 runs of CESM-LE. Two different grids have been considered for SSH and PSL. In the first case the runs extend from 60 S to 60 N, while for the PSL the models go from 10 to 90 N, for both cases the resolution is 1 degree. The reason for considering also the CESM-LE runs is that they give the possibility to explore how the variance of the KOE/NPTZ in one model (e.g. a fixed set of dynamics) responds to anthropogenic forcing when compared to the range of natural variability of the CESM-LE model. In the CMIP5-E, we cannot examine the changes in KOE/NPTZ variance against the natural variability in isolation because an important fraction of variability arises from the "model biases" in their representation of the KOE dynamics and variability. Therefore, the CESM-LE and CMIP-E provide us different but complementary insights into the climate change response of KOE/NPTZ variability.

2.4 Test to evaluate the significance of trends in variance in an ensemble

Here we develop a Monte Carlo approach to test if the changes in variance inferred from ensemble averaging multiple realizations of a timeseries are significant. Specifically, we use this test to estimate the significance of changes in variance found in the principal components of the climate model output. To calculate it we use 10,000 random pcs to compare the simulation with the real pc. These random pcs have been used as an input for the autoregressive model (AR1-model). The significance is then given by considering the difference in percentage between the real pc and the mean of the pcs calculated randomly.

3 Characterizing the North Pacific transition zone (NPTZ)

The impact of the physical climate variability of the KOE on the ecological dynamics of the NPTZ is evident from the large-scale co-variability between SSHa and CHL-a anomalies in the NPTZ. A pointwise correlation between satellite SSH and CHL-a anomalies (see methods for data sources) reveals a strong band of negative correlation ($R \sim -0.6$) extending from the Japan to California along the latitudinal boundaries of the NPTZ (Fig. 1b, see orange box). The NPTZ region is compatible to the one represented in the paper by Polovina et al. (2001), where the trajectories of loggerhead turtles are shown. The seasonal movements are to the North during summer, while they are to the South in Winter. The seasonal cycle is not the only influencing factor, the low frequency variability of the climate modes

Table 1 CMIP5 models

Model name	Institution
ACCESS1-0	Australian Community Climate and Earth System Simulator Coupled Model
ACCESS1-3	Australian Community Climate and Earth System Simulator Coupled Model
CESM1-BGC	National Science Foundation, Department of Energy, National Center for Atmospheric Research
CESM1-CAM5	National Science Foundation, Department of Energy, National Center for Atmospheric Research
CMCC-CMS	Centro Euro-Mediterraneo per I Cambiamenti Climatici
CMCC-CM	Centro Euro-Mediterraneo per I Cambiamenti Climatici
CanESM2	Canadian Centre for Climate Modelling and Analysis
EC-EARTH	The First Institute of Oceanography, SOA, China
FGOALS-g2	LASG, Institute of Atmospheric Physics, Chinese Academy of Sciences; and CESS, Tsinghua University
CSIRO-Mk3-6–0	Commonwealth Scientific and Industrial Research Organization in collaboration with the Queensland Climate Change Centre of Excellence
HadGEM2-CC	Met Office Hadley Centre
GISS-ES-R-CC	NASA Goddard Institute for Space Studies
GFDL-ESM2G	Geophysical Fluid Dynamics Laboratory
GFDL-ESM2M	Geophysical Fluid Dynamics Laboratory
GFDL-CM3	Geophysical Fluid Dynamics Laboratory
NorESM1-M	Institut Pierre-Simon Laplace
NorESM1-ME	Norwegian Climate Centre
Inmcm4	Institute for numerical mathematics
bcc-csm1-1-m	Beijing Climate Center, China Meteorological Administration
MPI-ESM-MR	Max Planck Institute for Meteorology (MPI-M)
MIROC-ESM	Japan Agency for Marine-Earth Science and Technology, Atmosphere and Ocean Research Institute (The University of Tokyo), and National Institute for Environmental Studies
IPSL-CM5A-MR	Institute Pierre-Simon Laplace
IPSL-CM5B-LR	Institute Pierre-Simon Laplace

has a great influence in establishing the migration direction of little turtles (Ascani et al. 2016). These species change their trajectories if the PDO is in positive or in negative phase. Changes in ocean advection related to the NPGO are also found to be critical in determining the zooplankton species distribution in the NPTZ, especially in the KOE region (Chiba et al. 2013).

A physical interpretation of the anti-correlation between SSH and CHL-a anomalies along the NPTZ and California Current System may be given by taking into consideration that the SSH in these regions tracks closely the upper ocean heat content because temperature effects generally dominates over salinity effects. Positive SSH anomalies are associated with warmer sea surface temperatures and higher heat in the upper ocean (Kelly et al. 2010), which in turn are indicative of downwelling conditions and/or reduced flux of nutrients from the deep ocean. The reduced nutrient content in regions of warmer SSTs/higher SSHa leads to less biologically productive waters and lower CHL-a content. Therefore, in the KOE the increase in SSH is associated to an increase of SST. The increase in stratification associated to the SST gradients lead to a decrease of nutrients and of the chlorophyll. A negative correlation in Fig. 1b between the SSH and the chl-a in the Kuroshio extension is then expected (Kouketsu et al. 2016; Storch and Zwiers 1999).

We also observe regions where the correlation between SSH and CHL-a anomalies is positive, especially along the Aleutian Islands and the Gulf of Alaska. In these regions, anti-cyclonic eddies are the primary mechanism supplying high nutrient waters from the coast into the open ocean through lateral advection and vertical mixing of nutrients is a minor control on the overall productivity (Di Lorenzo et al. 2013a, b).

To further examine the relation between physical and ecosystem variability we perform a more in-depth analysis of the covariance between SSH and CHL-a anomalies. A singular value decomposition (SVD) of the correlation matrix between SSH and CHL-a anomalies in the region on the NPTZ (black box in Fig. 1b, [− 220 to 140, 25 50]) reveals that this co-variability tracks the two dominant modes of North Pacific climate variability, the PDO and NPGO (Fig. 1c–f). We choose the SVD method as we are dealing with two different fields, the SSH and the CHL-a one. The SVD extracts structures that share most covariance between the two fields in a similar way in which the EOF's extract structures that explain most of the variance of an individual

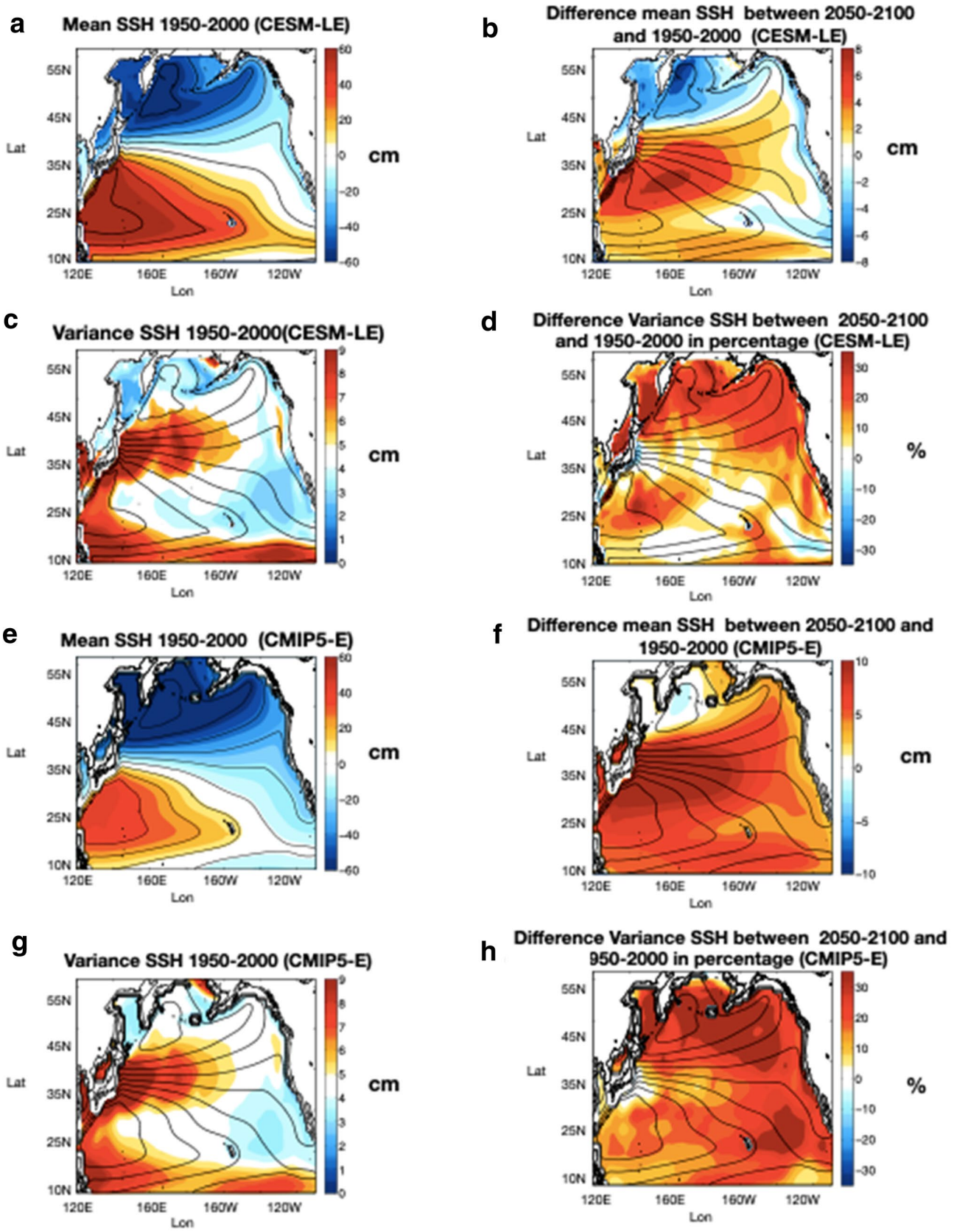
a
Mean SSH 1950-2000 (CESM-LE)
b
Difference mean SSH between 2050-2100 and 1950-2000 (CESM-LE)
c
Variance SSH 1950-2000(CESM-LE)
d
Difference Variance SSH between 2050-2100 and 1950-2000 in percentage (CESM-LE)
e
Mean SSH 1950-2000 (CMIP5-E)
f
Difference mean SSH between 2050-2100 and 1950-2000 (CMIP5-E)
g
Variance SSH 1950-2000 (CMIP5-E)
h
Difference Variance SSH between 2050-2100 and 950-2000 in percentage (CMIP5-E)
Lat
Lon
55N
45N
35N
25N
10N
120E
160E
160W
120W
cm
%

◂**Fig. 2** In (**a**) the mean SSH in the period 1950–2000 is explained, the black lines represents the contour of the SSH mean in this period. In (**b**) the difference between 1950–2000 and 2050–2100 SSH is calculated. In (**c**, **d**) the same is done but for the variance of the SSH. In (**e**–**h**) figures the same procedures have been followed but with CMIP5-E models. Units of SSH are in cm

variable. Consistent with previous findings (Taguchi et al. 2007) on the climate variability of the KOE, the spatial and temporal patterns of the first singular vector (SVD1) tracks the PDO (Fig. 1c, e) with a strong center of action in the KOE associated with a shift in the position of the NPTZ, while SVD2 tracks the NPGO with a North/South dipole characteristic of a change in strength of the NPTZ (Fig. 1d, f). The two modes are not only different for spatial structure but also for the quantity of variance explained, that is 25% in Fig. 1c and 15% in Fig. 1d.

4 Climate change projections of NPTZ, CESM-LE vs. CMIP5-E

4.1 Changes in mean circulation of the North Pacific Ocean

We now examine the output of long-term climate simulations to explore changes in mean and variance of the KOE circulation along the NPTZ under the climate warming scenario RCP8.5. Specifically, the CESM-LE large-ensemble (29 members) and an ensemble of CMIP5-E models (23 members) have been considered. The mean ensemble circulation for both the CESM-LE and the CMIP5-E (Fig. 2a, e) show a gyre circulation structure that is consistent with SSH satellite observations. To examine how and if the mean circulation changes under anthropogenic forcing, the difference of the mean SSH 2050–2100 minus 1950–2000 (Fig. 2b for CESM-LE, Fig. 2f for CMIP5-E) has been computed. Before calculating the means, a constant equal to the average SSH of the entire Pacific has been subtracted to the SSH. In both ensembles, we find a meridional dipole structure with amplitudes changes ~ 13% of the mean, which projects onto an intensification and northward shift of the mean KOE gradient region.

To better understand the relation between changes in mean circulation of the ocean and the atmospheric forcing we examine the Sea Level Pressure (SLP) fields in both the CESM-LE and the CMIP5-E ensemble. Figures 3a, e show the mean SLP for the period 1950–2000 for CESM-LE and CMIP5-E, while Fig. 3b, f shows the difference SLP 2050–2100 minus 1950–2000. In the SLP difference maps we find a weakening and Northward shift of the Aleutian Low with center of action at 40 ° N. In the CMIP5-E and in the CESM-LE outputs, we also find a reduction of SLPa over the polar latitudes (> 50 ° N). These results are consistent with previous studies (Yang et al. 2016; Gillett and Fyfe 2013) documenting a climate change signature in SLP similar to the positive phase of the Northern Annular Mode with a poleward shift of the Westerlies linked to negative SLP over high latitudes and positive SLP at mid-latitudes. The difference in mean SLP between present and future climate are not necessarily significant in terms of absolute value given that the amplitude of the changes is less than the standard deviation (e.g. compare panel f and g in Fig. 3). However, the changes in the large-scale gradients of SLPa are significant. For example, in the CESM-LE, the gradient between the sub-tropical gyre region (e.g. 50° N) and the pole (e.g. 75° N) changes by ~ 10 Pa (Fig. 3b), which corresponds to a significant fraction (35%) of the mean gradient of ~ 35 Pa (Fig. 3a). These changes in the gradient impact the surface winds and ocean circulation. Specifically, the enhanced positive gradient from the subtropical gyre region to the poles leads to stronger downwelling in the subtropical pacific which leads to higher SSH in the subtropics and lower SSH in the subpolar gyre. Consistent with these changes in downwelling/upwelling conditions, the ocean circulation difference maps inferred in the SSH show a poleward shift and intensification in the NPTZ during the period 2050–2100.

This climate change signature is also evident by performing an EOF analysis of the ensemble mean SSH of the CESM-LE and CMIP5-E (Fig. 4). The first EOFs reveal again the same dipolar pattern (Fig. 4a, c) and the first principal components is characterized by a strong trend developing at the end of the 21th century (Fig. 4b, d). This finding is consistent with previous studies with CMIP5-E models suggesting that the KOE is warming and shifting poleward as a response to anthropogenic forcing (Yang et al. 2016). Some studies attribute these changes to either an increase in baroclinicity, or an expansion of the Hadley Cell with a poleward shift in the Westerlies (Vallis et al. 2015; Deser et al. 1999). An alternative explanation has been done by Chen et al. (2008) for which the increase in temperature leads to a change in critical latitude of the eddies. As a consequence, there is a poleward shift of eddy momentum flux and also of the Westerlies.

The climate spatial trends in the mean SLP changes emerge also in the first EOF of SLPa where the trends have not been removed (Fig. 4c for CESM-LE and Fig. 4g for CMIP5-E). However, the ensemble means first principal component in CESM-LE and CMIP5-E (Fig. 4b, f) do not show strong trends because the changes in mean SLP are weak compared to the standard deviation of the field.

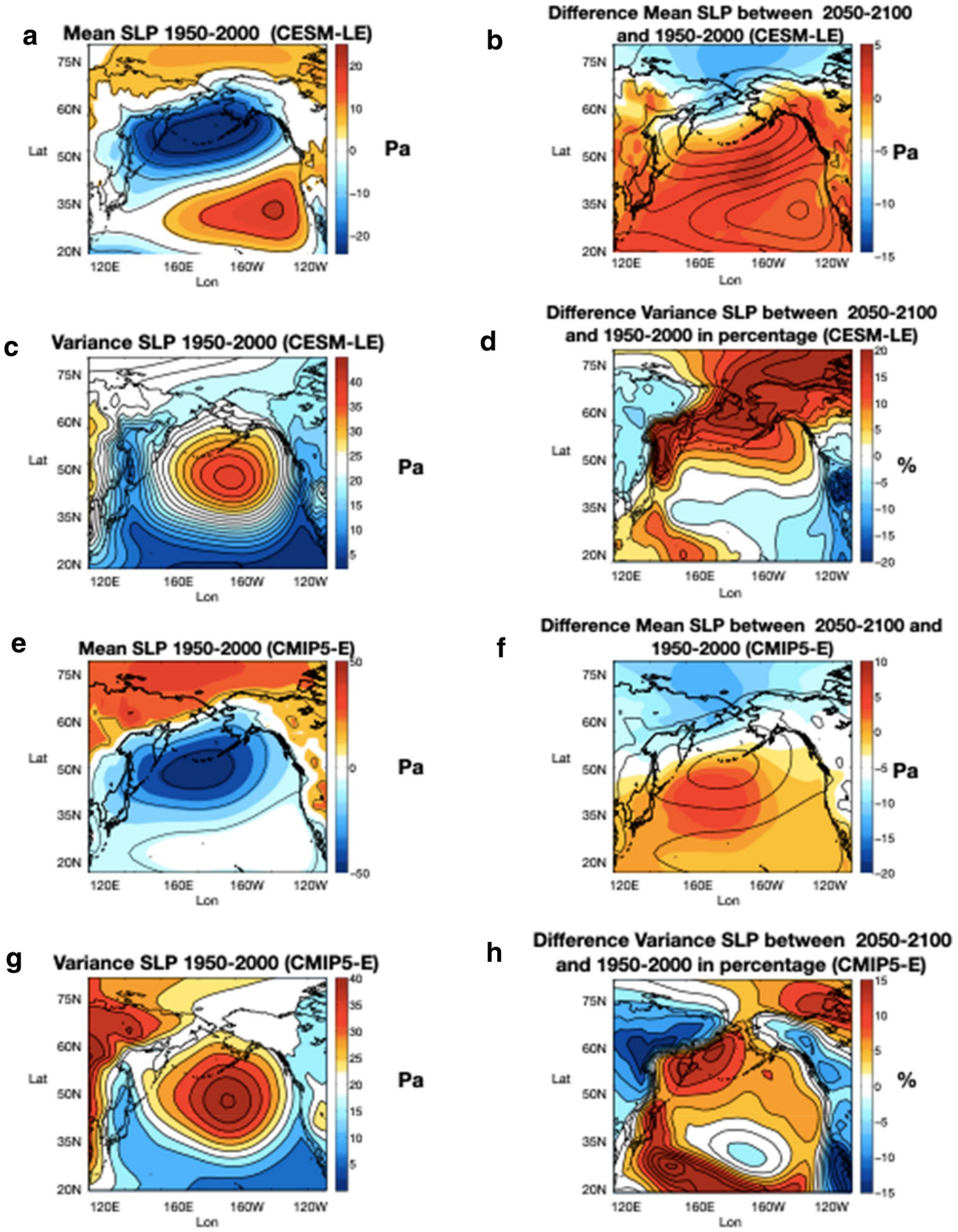

Fig. 3 In (**a**) the mean SLP in the period 1950–2000 is explained, the black lines represent the contour of the mean SLP in this period. In (**b**) the difference 1950–2000 and 2050–2100 SSH is calculated. In (**c**, **d**) the same is done but for the variance of the SLP. In (**e**–**h**) figures the same procedures have been followed but with CMIP5-E models. Units of SLP are in Pascal

4.2 Changes in the variability of the NPTZ

Both the CESM and CMIP5 ensemble capture the structure of the mean spatial variance of SSHa over the North Pacific with strong values in the KOE region (Fig. 2c, g). To quantify how the variability of the NPTZ changes under anthropogenic forcing, we compute the difference in the mean spatial variance for the period 2050–2100 minus 1950–2000 for both the CESM-LE (Fig. 2d) and CMIP5-E (Fig. 2h) ensemble. Both the CMIP5-E and the CESM-LE runs gives a significant increase in the mean SSH that is associated with a lower increase of variance in the Kuroshio extension region. The increased SSH gradient (Figs. 2b and 3b) works to intensify the midlatitude westerlies resulting in an increasing wind stress curl field. As the subtropical gyre increases the SSH mean, as we can see from the southern recirculation gyre, the corresponding intensification of poleward heat transport reverse this effect.

To further understand the dynamics underlying the changes in variance, and how it impacts the NPTZ, we decompose the variance using an EOF analyses. Specifically, we consider the spatial domain [215 –140 W; 30 –50 N] that was used to extract the two dominant modes of SSHa-CHL-a co-variability (Fig. 1c, d) associated with a shift in positions and changes in intensity of the NPTZ circulation. Prior to the computation of the EOFs we remove the anthropogenic signals in the CESM-LE and CMIP5-E (see methods) in order to focus on changes in the variability that are not influenced by the anthropogenic trends. For each model realizations we compute the first two modes and align the signs of each mode so that the spatial expressions are consistent in sign with that of the observations in Fig. 1. We then take the ensemble mean of the spatial patterns for the CESM-LE and CMIP5-E simulations. We find the spatial structure of the first two modes of SSHa, in both CESM-LE (Fig. 5) and CMIP5-E (Fig. 6), track closely the modes derived from observations (Fig. 1c, d), suggesting that the climate models capture realistically the dominant structures of SSHa variance over the NPTZ region. The first SSHa mode reveals a strong pole over the NPTZ region that is consistent with a shift in the axis of the KOE (Fig. 1c) and tracks the PDO mode of the models (e.g. In supplemental materials the PDO index has been computed by using the SSH anomalies and compared with the same index with the SST anomalies). The second mode reveals a meridional dipole associated with a change in the strength of NPTZ gradient and tracks the NPGO indices in each model.

We now explore the changes in variance in the two dominant modes of NPTZ variability and test if there are any significant changes over the period 1920–2100. For the CESM-LE, we begin by taking the absolute value to the individual PC1 realizations (Fig. 5c, gray line), we then average the PC1s together (Fig. 5c, ensemble mean is the black bold line) and fit a quadratic trend model (Fig. 5c, green line, $y(t) = at + bt^2$) to estimate the long-term changes in variance. The percentage change in variance with respect to 1920 values is found by scaling the trend by the value on January 1920 and multiplied by 100 (Fig. 5e, green line). The same procedure is repeated using only winter (Fig. 5e, blue line) and summer (Fig. 5e, red line) values to understand if there are seasonal dependences in trend in the variance. In the case of CESM-LE PC1, we find a significant increase in the total variance of about 20% by 2100, with about 25% in the summer and ~ 10% in the winter (see below for the significance test). The second mode of the CESM-LE also shows very significant increase in variance (Fig. 5c, f) with a predicted amplification of about 30% by 2100.

Test of significance for the ensemble trend in variance To assess if the trends of variance in the ensemble average are significant (e.g. green line, Fig. 5c), we develop a Monte Carlo approach that simulates the trend estimation process used to derived the ensemble trend in variance shown in Fig. 5 (green line). Specifically, we generate 10,000 random realizations of the ensemble trend (gray spread, Figs. 5e and 6e). Each random trend line is generated by applying the quadratic trend fit on 30 random PC1s red noise timeseries that have the same autocorrelation as in the original 30 PC1s of the CESM ensemble. This test is also repeated for estimating the significance of the PC2 trends in variance (gray spread, Figs. 5f and 6f).

To understand if the predicted changes in variance from the CESM ensemble are robust, we perform the same trend analyses for the CMIP5-E. We find that the trend in variance for PC1 is confirmed in the CMIP5-E with a total variance increase ~ 10% (Fig. 6e). However, for PC2, the CMIP5 ensemble does not predict a significant change in variance (Fig. 6f). The lack of a significant trend in the PC2 running variance reveals an important discrepancy between the CMIP5-E and the CESM-LE scenario, which may indicate a high level of uncertainty emerging from the model's inability to reproduce a consistent NPGO dynamics e.g. Furtado et al. (2011).

5 Atmospheric forcing of the NPTZ variance: CESM-LE vs. CMIP5-E

The NPTZ variability of the KOE SSHa modes is strongly linked to the atmospheric forcing of the North Pacific. We proceed by doing a correlation analysis between the detrended SLP anomalies with SSH_PC1 and SSH_PC2 to extract the atmospheric forcing patterns. As we did in the previous section, before calculating the means, a constant equal to the average SLP of the entire Pacific has been subtracted from the SLP. In both the CESM and CMIP5 ensembles, the ensemble mean correlation pattern associated with SSH_PC1 is characterized by a strong single pole

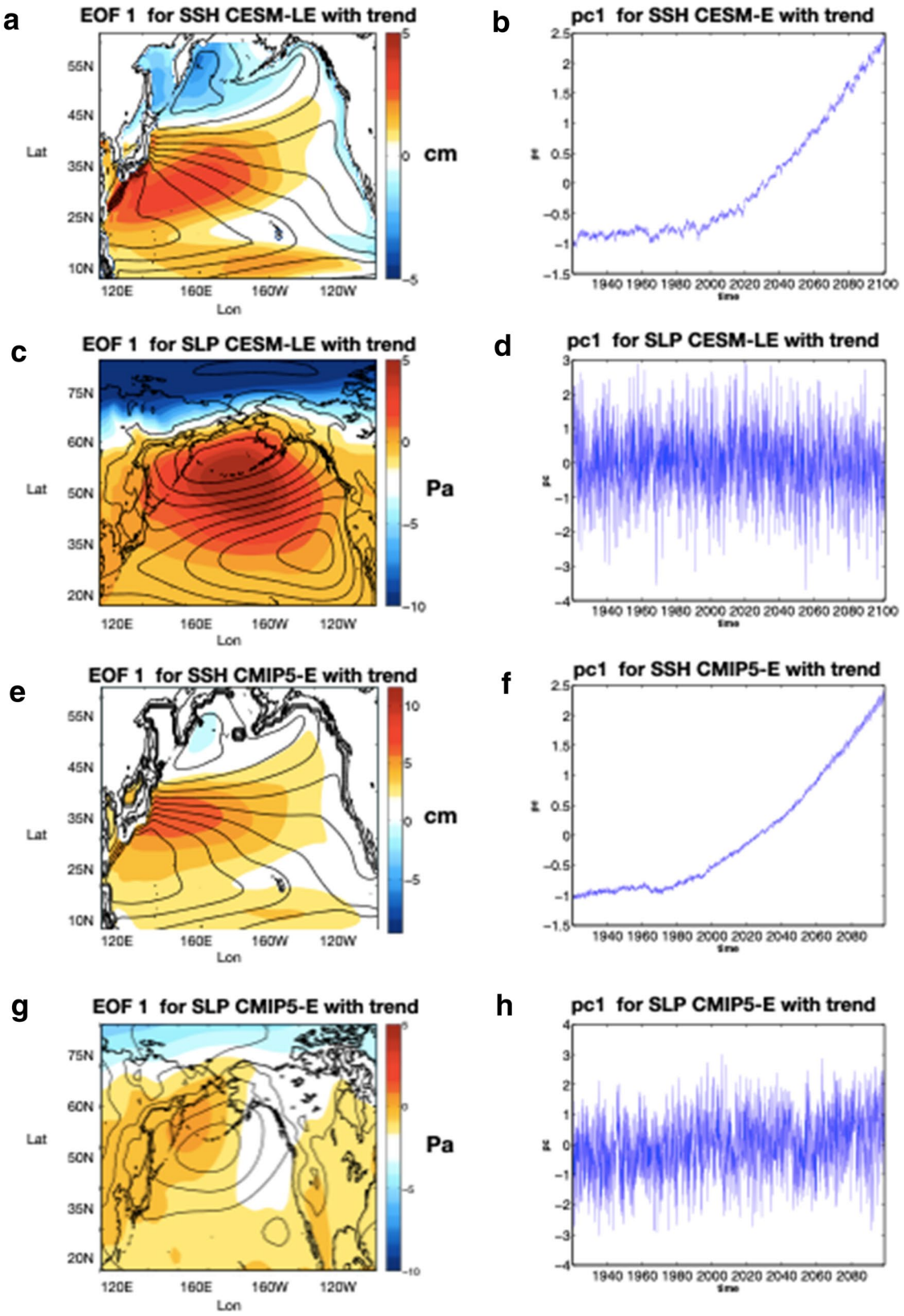

Fig. 4 In (**a**, **b**) we display the first EOFs with trend with the associated pc. This gives a clear increasing trend. In (**c**, **d**) the same EOF is calculated for the SLP with associated pc that does not give an increasing scenario. We repeat the same procedure with CMIP5-E models in f(**e**–**h**). Units of SSH are in cm, while for the SLP. Units are in Pa

over the North Pacific that sits between the North Pacific High and Aleutian Low (Figs. 7a and 8a, the black contour lines represent the mean values of SLP between 1950 and 2000). In contrast, the SSH_PC2 correlation pattern in the SLPa (Figs. 7b and 8b) exhibits a meridional dipole structure with the center of action close to the mean locations of the Aleutian Low North Pacific High. We refer to these two dominant SLPa structure as the atmospheric forcing patterns of SSH_PC1 and SSH_PC2.

To further explore the changes in SLP variability we extract a time index associated with the SLPa forcing patterns. These time series are calculated by projecting the SLPa of each run onto its corresponding forcing pattern (CORR1(x,1) and CORR2(x,1)).

$$SLP_{index}(t) = SLPa'(t,x) * CORR1(x,1) = \int SLP_a(t,x) * CORR1(x,1)dx \quad (2)$$

$$SLP_{index2}(t) = SLPa'(t,x) * CORR2(x,1) = \int SLP_a(t,x) * CORR1(x,1)dx \quad (3)$$

Similar to the running variance evaluation performed for the SSHa PC1 and PC2, we estimate the change in variance of the SLPa forcing patterns. Figure 7c, d and 8c, d show the absolute value of the SLP forcing timeseries for each individual model run, while the black thick line is the ensemble mean. We fit a quadratic trend model to the ensemble mean to measure how the standard deviation is changing with respect to 1920s values (green line in Figs. 7e, f and 8e, f). A Monte Carlo approach (see Methods) has been used to test the significance of the quadratic trend. We find that the SLPa forcing pattern associated with SSHa_PC1 in the CESM-LE has a positive trend with a significant increase of ~ 15% by 2100 while CMIP5 shows a 10% increase. In the CMIP5 ensemble the trends in variance are positive but do not exceed the threshold for significance. These trends are also evident in the seasonal means using January–February-March (JFM) and June-July–August (JJA) (blue and red curve in Figs. 7e and 8e).

The SLPa forcing pattern associated with SSH_PC2 (7f and 8f) has an increasing trend for both the CESM-LE and the CMIP5-E models. However, the Monte Carlo significance test suggests that these changes are not very significant.

5.1 Correlation SLP forcing index with SSH_PC1 and SSH_PC2

To further understand and verify the relation between the SLPa forcing timeseries and the SSHa PCs we develop a simple statistical model that relates changes in SSHa to SLPa forcing,

$$\frac{dSSH_{PC1}(t)}{dt} = SLPa_{Forcing1}(t) - \gamma SSH_{PC1}(t) \quad (4)$$

Following the approach of Frankignoul and Hasselman (1977), Eq. 4 represents a simple model of climate system where the rate of change of the SSHa is forced by the atmospheric SLPa and decays back to zero with a damping time scale defined by $1/\gamma$. Negative feedback leads to an asymptotic balance between the random forcing and the feedback damping yielding to a statistically stationary response. If we consider SLPa = [SLPa] + $SLPa_{Forcing1}(t)$, in an equilibrium condition the mean value of SLPa can be consider negligible. In this way the response of the climate system to the continuous random forcing can be represented as a first order autoregressive model (AR-1 model). At the same time the meaning of the coefficient γ can also be seen by looking at the autocorrelation of the red noise, $r(\tau) = \exp\left(-\frac{\tau}{T}\right)$, τ is the time lag while γ represents the damping rate given by the inverse of the autocorrelation decay time T.

We analyze the influence of the forcing factor represented by the $SLPa_{Forcing1}(t)$ on the SSH_PC1 by calculating the correlation between the two indices. In Fig. 9a, c the ensemble mean correlation has been done for the SSH_PC1 and the forcing index obtained from integration of SLP_PC1. A correlation of 0.71 for CESM and 0.49 for CMIP5 has been obtained. To estimate the significance of the correlations the PDF of cross-correlation coefficients is represented in the same figures. To build the PDF we examine the correlation of 1000 random pairs that have the same autocorrelation of the two-time series considered. In Fig. 9b, d the SLP forcing index from model (4) is calculated with SLP_PC2. In this case the ensemble mean correlation of the index with SSH_PC2 gives a correlation of 0.57 for CESM-LE and 0.39 for CMIP5-E.

To further understand the relation between the atmospheric forcing and the KOE, we adopt a lag correlation analysis proposed by Frankignoul et al. (1998). The essence of this approach is to examine the correlation between an atmospheric variable, the SLPa field, and the SSH_PC1 (Supplemental Materials) with a lag that is longer than the intrinsic atmospheric timescale (~ 2 month, Deser et al. (2007). The resulting correlation maps show significant correlation patterns similar to Figs. 7a and 8a when the SLPa patterns lead the SSHa PCs by 12 months. This confirm that the SLP acts as a forcing of the KOE SSH and NPTZ. To explain this leading time, we can consider that when the Aleutian Low intensifies (positive phase of the PDO) it cools the Central North Pacific and generates SSH anomalies through Ekman divergence. Kwon et al. (2010). It also has been found by other studies (Ceballos et al.

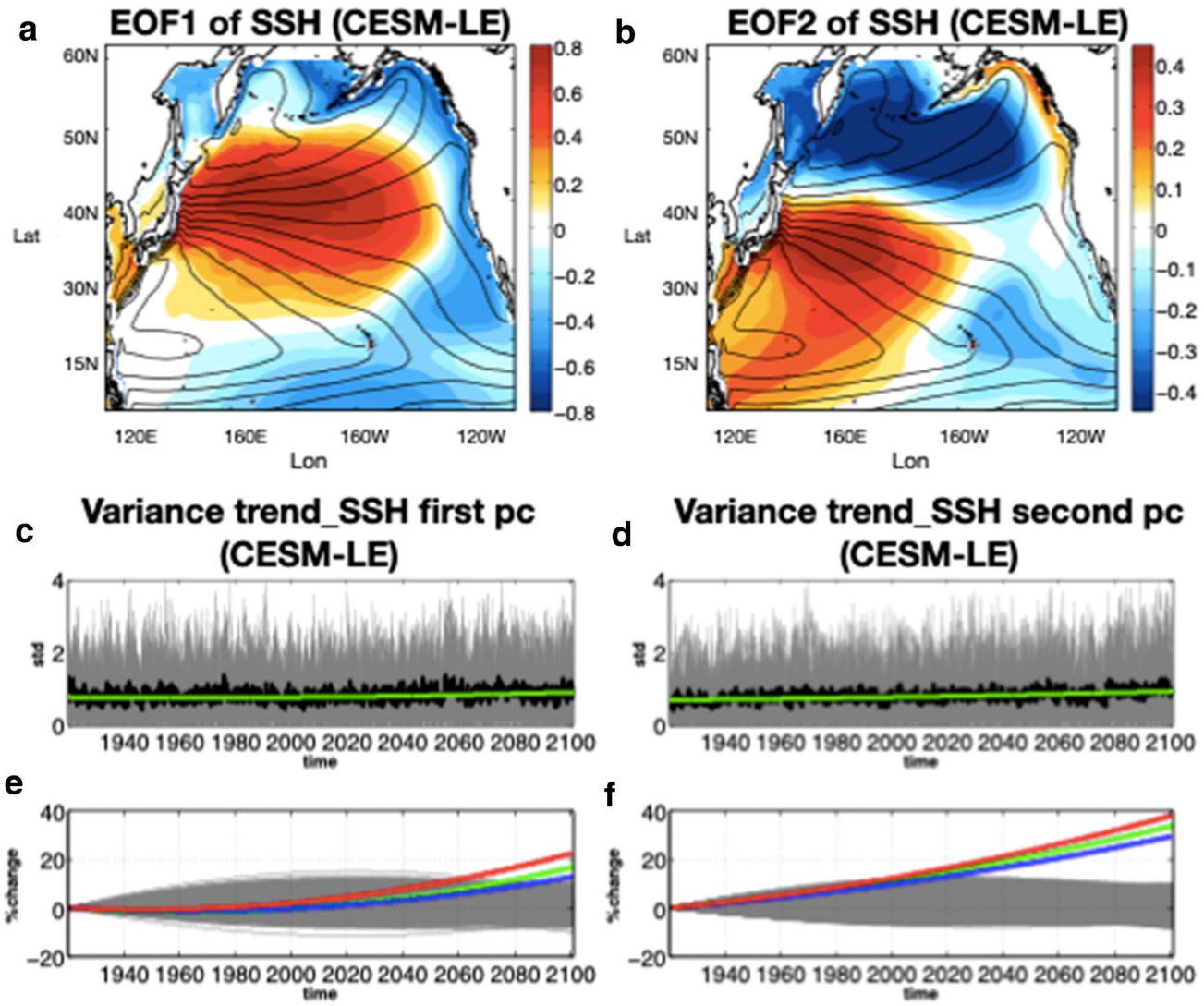

Fig. 5 In (**a**, **b**) the first and second correlation patterns for the SSH anomalies are represented. In this case the anomalies have been detrended. The trend in the variance corresponding to the first pattern is displayed in (**c**). The principal components for each single runs are the grey part while and the mean pc in in black. The red line is the increase for just the summer season, while the blue line regards the winter season. In (**d**, **f**) the same is done but using second pattern of correlation. In this case the CESM-LE runs are taken into consideration. Units of SSH are in cm

2009) that the Rossby waves generated by NPO induced SLP anomalies can have an impact in the KOE. The time of wave propagation give rise to the time lag of 6–12 month.

6 Summary and discussion

The presence of strong chlorophyll gradients makes the NPTZ a region of great importance for ecosystem dynamics. Changes in the location and amplitude of the chlorophyll gradient are strongly connected to changes in the KOE dynamic circulation. This is evident from the dominant modes of covariability between SSHa and chlorophyll-a in the KOE region in satellite observations (Fig. 1). The first mode represents a meridional shift in location of the KOE/NPTZ and tracks the PDO, whereas the second mode has a dipole structure and describes an intensification of the KOE mean circulation and the NPTZ.

To understand the impact of anthropogenic forcing on the NPTZ, we examine the projected changes in the characteristics of the KOE physical modes using the Community Earth System Model Large Ensemble (CESM-LE) and 23 CMIP5-E models. We consider the change in SSH mean and variance between two time periods, 1950–2000 and 2050–2100 (Figs. 2 and 3). The SSH mean difference map gives a meridional dipole structure that projects onto an

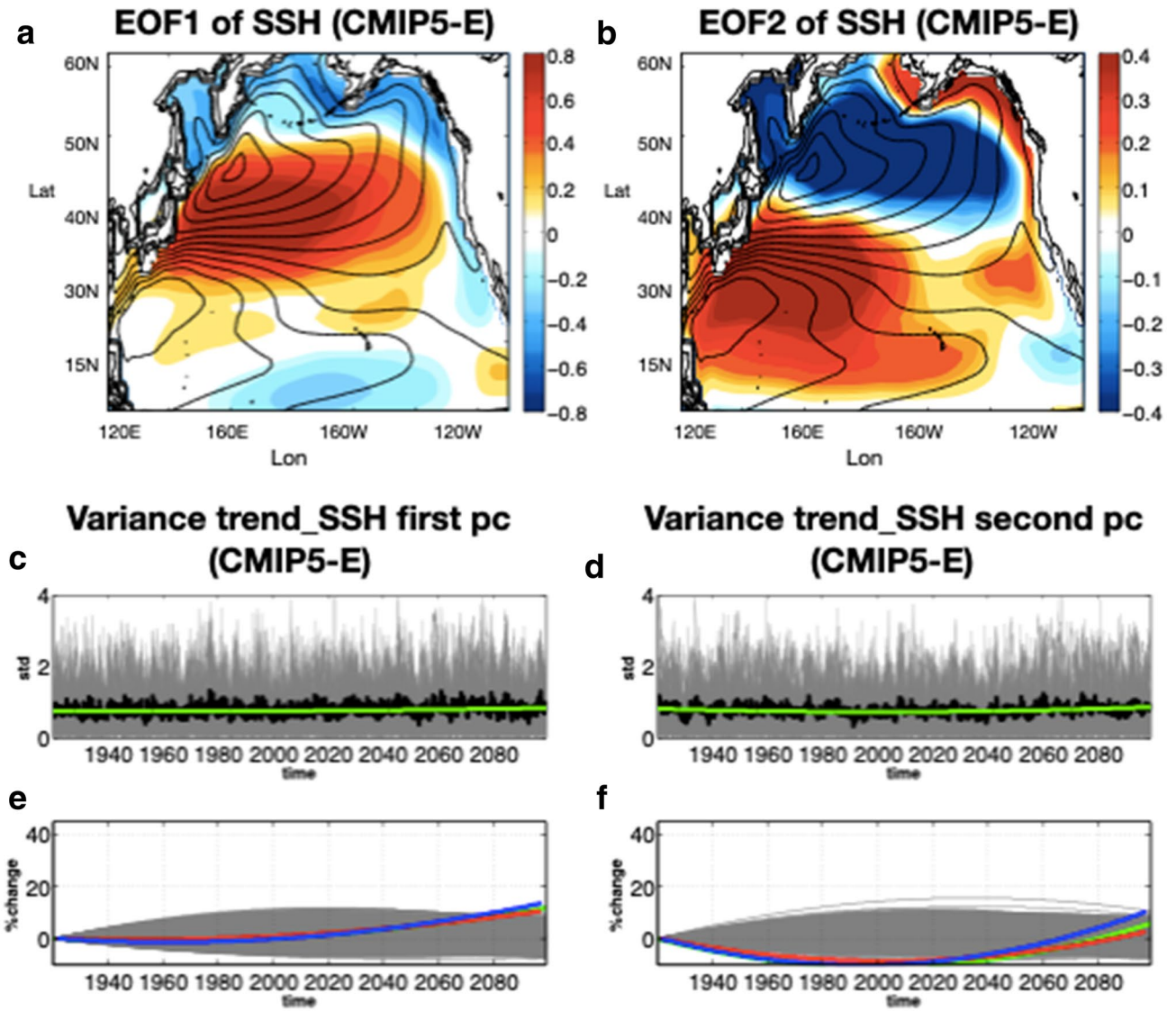

Fig. 6 In (**a**, **b**) the first and second correlation patterns for the SSH anomalies are represented. In this case the anomalies have been detrended. The trend in the variance corresponding to the first pattern is displayed in (**c**). The principal components for each single runs are the grey part while and the mean pc in in black. The trend of the variance is given by the green line. In (**e**) the percentage increases is represented. The red line is the percentage increase for just the summer season. In (**d**, **f**) the same is done but using the second pattern of correlation. In (**e**, **f**) the grey part is inductive of the significance test performed. In this figure the CMIP5 models are taken into the consideration. Units of SSH are in cm

intensification and Northward shift of the KOE and NPTZ. The poleward shift is also associated with a Southeastward movement of the Aleutian Low as revealed from the SLP mean difference maps.

A shift in the North Pacific atmospheric circulation has been previously examined. Vallis et al. (2015) found a correlation between the expansion of the Hadley cell and the poleward shift of the Westerlies and the corresponding ocean circulation imprint. An alternative explanation is given by Chen et al. (2008), which argue that as a consequence of global warming the phase speed of midlatitudes atmospheric eddies increases. This leads to a poleward shift of the eddy-momentum flux and, as a consequence, of the Westerlies.

Several studies have recognized that changes in climate variance, rather than changes in the mean, are a better predictor of phase and regime shift in a variety of oceanic systems (Sydeman et al. 2013). We have explored the changes in the NPTZ variance by examining the two dominant modes of detrended KOE SSHa (Figs. 5 and 6) in the CESM-LE and CMIP5 ensemble. A Monte Carlo test has been done to test the significance of the trend. The CESM-LE suggests a 20% increase in the SSHa of SSH_PC1 while for the

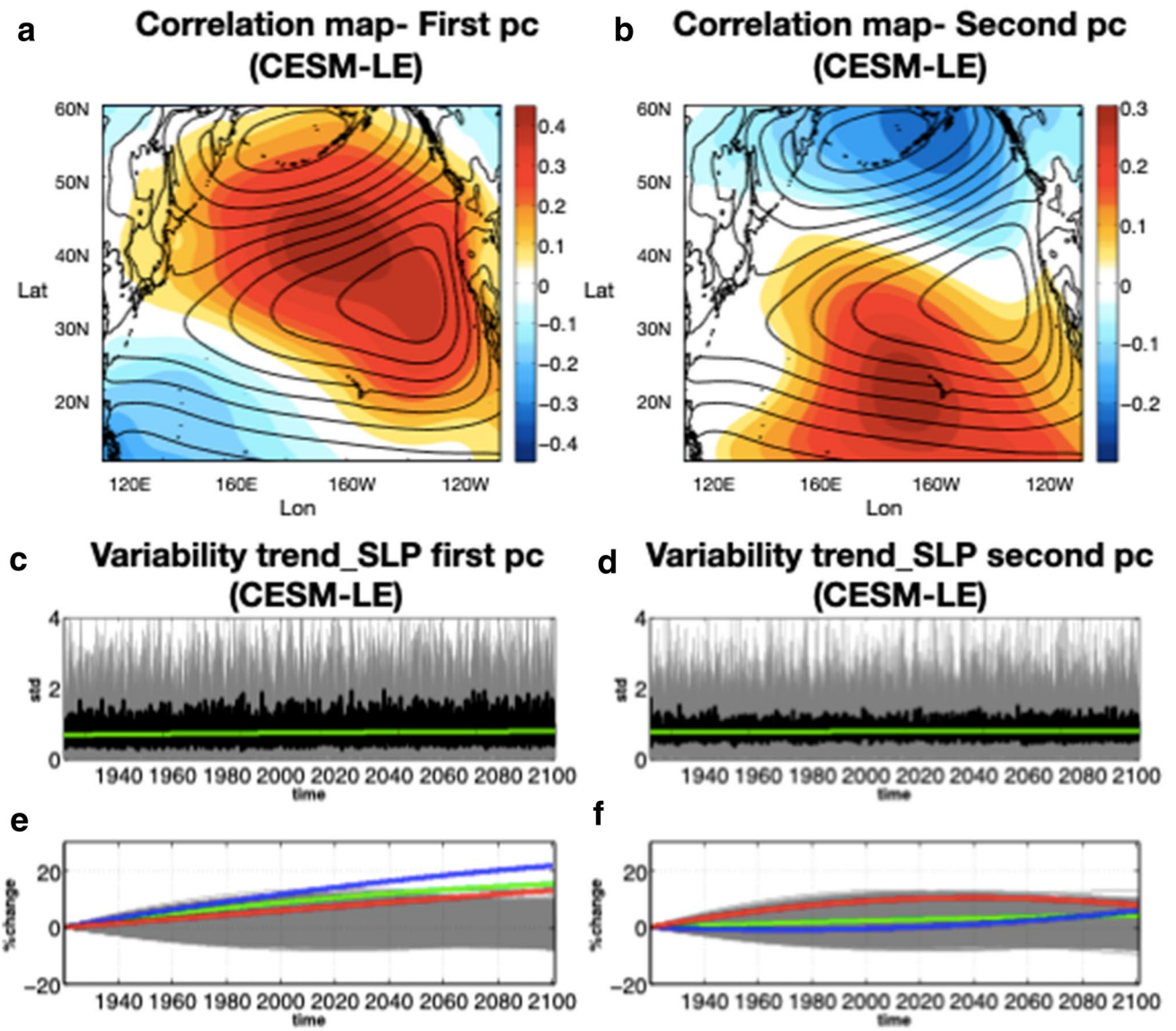

Fig. 7 In (**a**, **b**) the first correlation patterns for the SLP anomalies over the first pc of the SSH is represented. The trend in the variance corresponding to the first pattern is displayed in (**c**). The principal components for each single runs are the grey part while and the mean pc in in black. The red line is the increase for just the summer season, while the blue line regards the winter season. In (**b**) the second correlation pattern associated to the SLP anomalies over the second of pf of SSh is displayed. The trend in the variance corresponding to the first pattern is described in (d) while the associated percentage increases is in (**f**). The grey part is in (**e**, **f**) described the significance test performed. In this case the CESM runs are taken into consideration. Units of SSH are in cm

CMIP5-E models the increase is almost 15%. We found that the increase in SSH variance is associated to trends in the variability of the corresponding SLP forcing patterns (e.g. SLP_PC1) (Figs. 7 and 8). For SSH_PC2, the CESM-LE predicts a very significant trend in variance with changes up to 30–40%. However, in the CMIP5-E this trend is not as significant, and the corresponding forcing patterns in SLP do not exhibit clear trends (e.g. SLP_PC2). This may indicate that changes in the variance of the CESM-LE second mode, and to some degree of CMIP5-E, are driven by internal ocean processes linked to the changes in the mean circulation.

To further examine the relation of the SSHa modes (SSH_PC1 and SSH_PC2) to atmospheric forcing in the KOE we apply a simple auto-regressive model of order 1 forced by indices of the SLPa forcing patterns (SLP_PC1 and SLP_PC2) (Eq. 4). The reconstructions of SSH_PC1 in the CESM-LE gives a correlation of 0.71 while for the CMIP5 the values are lower, 0.45. Lower correlation values are found in the reconstruction of SSH_PC2 with a correlation of 0.57 for the CESM-LE and 0.39 for CMIP5-E. The

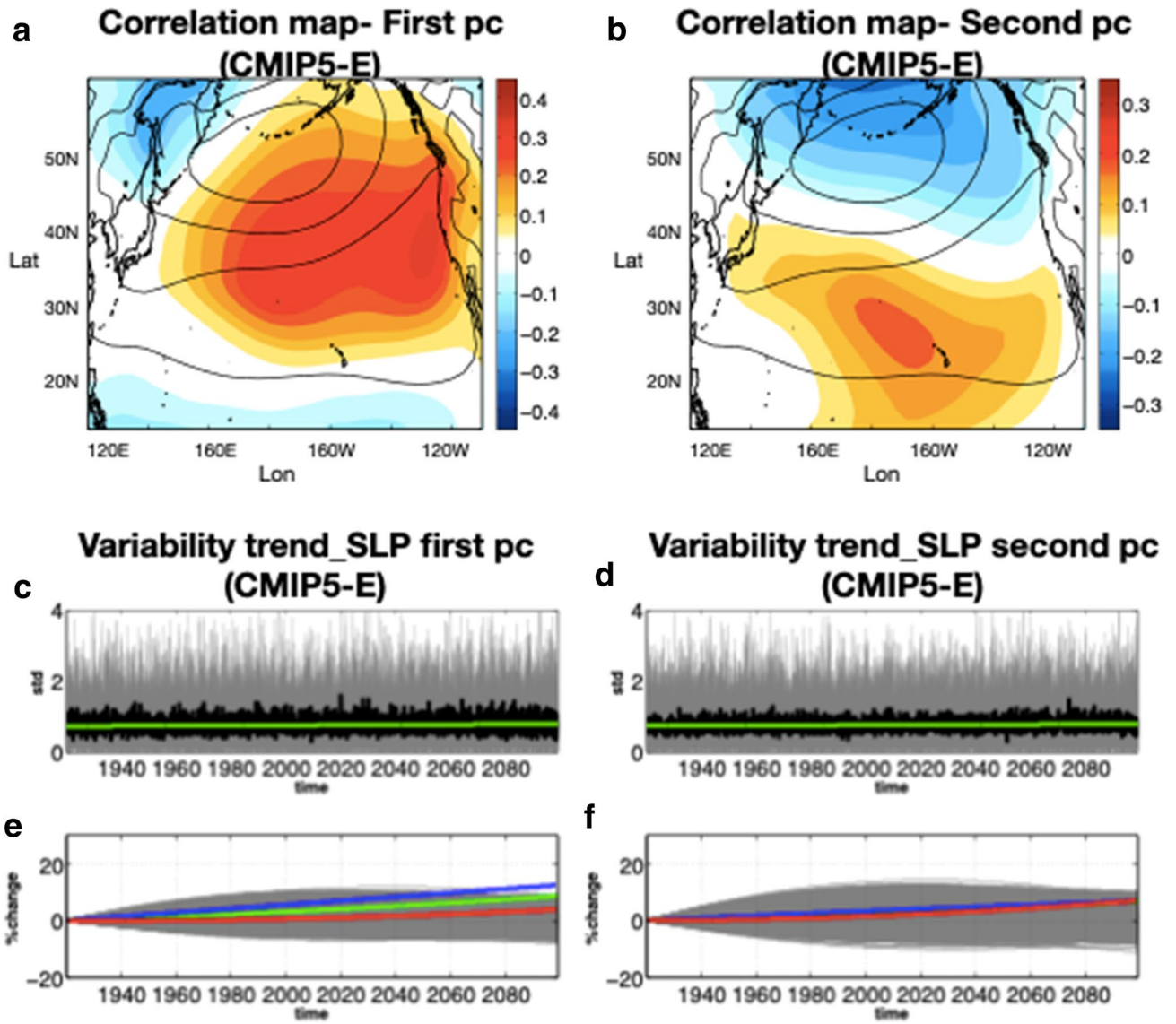

Fig. 8 In (**a**) the first correlation patterns for the SLp anomalies over the first pc of SSH is represented. The Trend in the variance corresponding to the first pattern is displayed in (**c**). The principal components for each single runs are the grey part while and the mean pc is in black. The trend of te variance for just the summer season, while the blues line regards the winter season. In (**b**) the second correlation pattern associated to the SLP anomalies over the second pf of SSH is displayed. The trend in the variance corresponding to the first pattern is described in (**d**) while. The associated percentage increase is in (**f**). The grey part in (**e**, **f**) describe the Significance test performed. In this case the CMIP5-E models are taken into consideration. Units of SSH are in cm

weaker correlation in the reconstruction of the second SSHa mode further confirms the role of internal ocean dynamics in controlling its variability.

The changes in KOE circulation and NPTZ identified in this study have several biological implications. In addition to the co-variability between the SSHa and CHL-a, which can be considered a proxy for primary productivity, the variability of the NPTZ is linked to higher-trophic ecosystem dynamics. For example, changes in the intensity of the KOE circulation, captured by the second SSHa mode, have been linked to alternation of zooplankton species found in the NPTZ (Chiba et al. 2009a, b). Similarly, meridional shift in the axis of the NPTZ associated with changes in the AL intensity, captured by the first SSHa mode, are linked to changes in overall biomass of zooplankton lower biomass during stronger AL, Nakata et al. (2001) and changes in migration patterns marine turtles (Ascani et al. 2016). While these links between the NPTZ variability and marine ecosystem dynamics clearly indicate that marine populations respond to the SSHa modes of variability, it remains unclear how a trend in the variance of these modes will untimely impact ecosystem function. Rising trends in climate variance

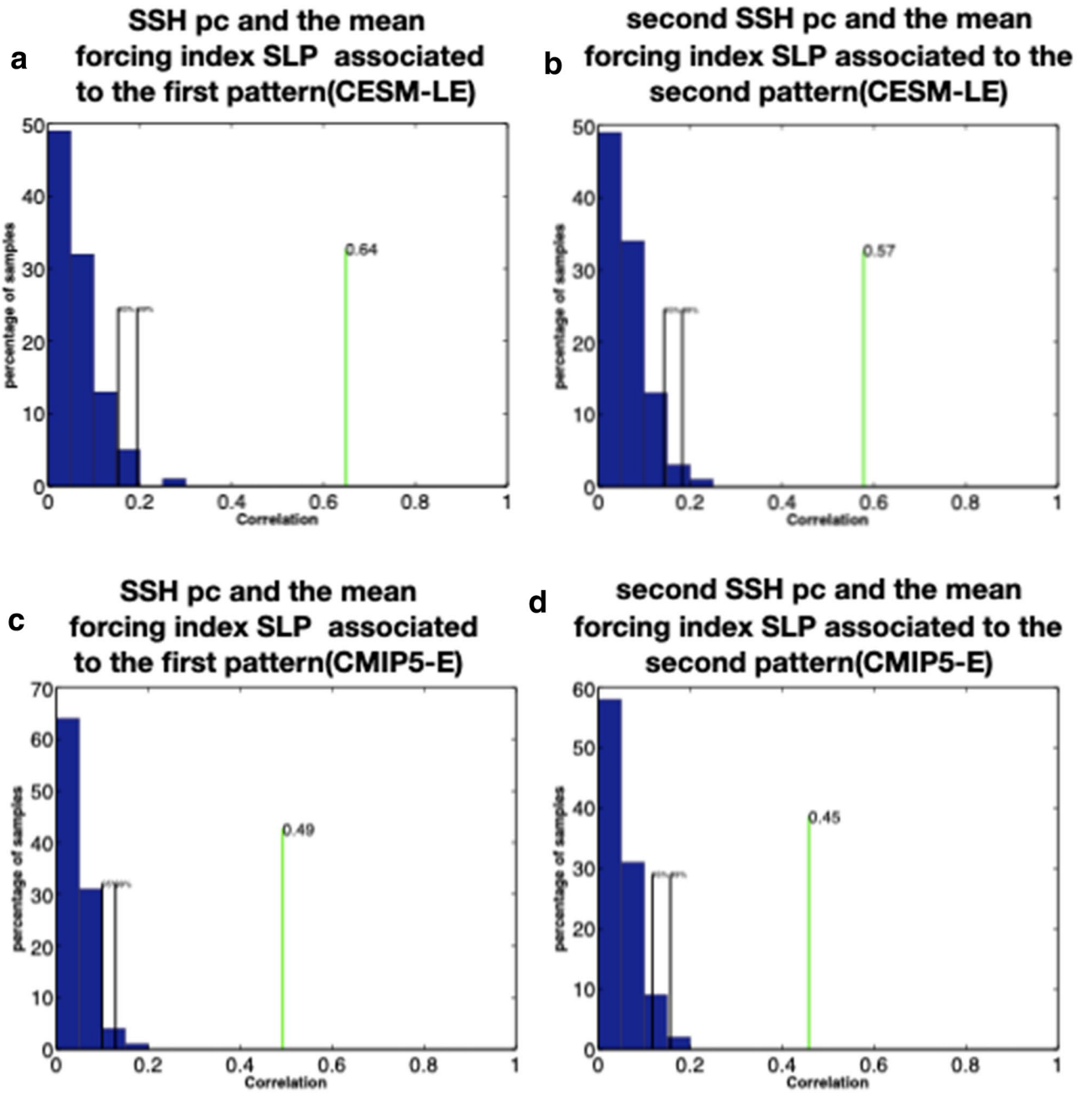

Fig. 9 In this case we consider the response of the climate system to continuous random forcing and its correlation with the first and second pc of SSH. Inf Fig. (**a**, **b**) the correlation between the SLP forcing index and the SSh ensemble mean first and second pc is represented. In this case the CESM-LE output has been used. In (**c**, **d**) the same figures have been done with the CMIP5-E models. We obtain a correlation a little higher in the CESM-LE case

are accompanied with rising levels of synchrony (e.g. covariability) (Black et al. 2018). Such a rise in synchrony may destabilize ecosystem and expose populations to higher risks of extinction by reducing the so called "portfolio effect". Specifically, when marine populations respond more synchronously to the same perturbations, they become less resilient and more susceptible to sudden collapses with disruptions of the ecosystem services they provide e.g. (Moran 1953).

Although more studies are required to confirm the link between changes in NPTZ variance and anthropogenic forcing, consistent with other recent studies (Sonnewald et al. 2018; Joh and Di Lorenzo 2017], the analyses of the climate models ensemble presented in this study provide

statistical evidence that climate change is impacting not only the mean structure of the North Pacific circulation but also its variance.

Supplementary Information The online version contains supplementary material available at https://doi.org/10.1007/s00382-021-05677-0.

Acknowledgements The work is supported by the OSE (Ocean Science and Engineering) funds of the Georgia Tech University, and support of the Department of Energy (DOE) grant DE-SC0019418. We also thank Dr. Liguori for helping with the processing of the CESM-LE data archive.

References

Ascani F, Van Houtan KS, Di Lorenzo E, Polovina JJ, Jones TT (2016) Juvenile recruitment in loggerhead sea turtles linked to decadal changes in ocean circulation. Glob Change Biol 22(11):3529–3538. https://doi.org/10.1111/gcb.13331

Black B, van der Sleen P, Di Lorenzo E et al (2018) Rising synchrony controls western North American ecosystems. Glob Change Biol 24:2305–2314. https://doi.org/10.1111/gcb.14128

Ceballos LI, Di Lorenzo E, Hoyos CD, Schneider N, Taguchi B (2009) North Pacific gyre oscillation synchronizes climate fluctuations in the Eastern and Western boundary systems. J Clim 22(19):5163–5174. https://doi.org/10.1175/2009jcli2848.1

Chen G, Lu J, Frierson DM (2008) Phase speed spectra and the latitude of surface westerlies: interannual variability and global warming trend. J Climate 21:5942–5959. https://doi.org/10.1175/2008JCLI2306.1

Chiba S, Sugisaki H, Nonaka M, Saino T (2009a) Geographical shift of zooplankton communities and decadal dynamics of the Kuroshio-Oyashio currents in the western North Pacific. Glob Change Biol 15:1846–1858

Chiba S, Sugisaki H, Nonaka M, Saino T (2009b) Geographical shiftof zooplankton communities and decadal dynamics of the Kuroshio-Oyashio currents in the western North Pacific. Glob Change Biol 15:1846–1858

Chiba S, Lorenzo E, Davis A, Keister JE, Taguchi B, Sasai Y, Sugisaki H (2013) Large-scale climate control of zooplankton transport and biogeography in the Kuroshio-Oyashio Extension region. Geophys Res Lett 40(19):5182–5187. https://doi.org/10.1002/grl.50999

Deser C, Alexander MA, Timlin MS (1999) Evidence for a Wind-driven intensification of the Kuroshio current extension from the 1970s to the 1980s. J Clim 12:1697–1706. https://doi.org/10.1175/1520-0442(1999)012%3c1697:EFAWDI%3e2.0.CO;2

Deser C, Tomas RA, Peng S (2007) the transient atmospheric circulation response tp North Atlantic SST and sea ice anomalies. J Climate 20:4751–4767. https://doi.org/10.1175/JCLI4278.1

Di Lorenzo E, Mantua N (2016) Multi-year persistence of the 2014/15 North Pacific marine heatwave. Nat Clim Change 6:1042–1047. https://doi.org/10.1038/nclimate3082

Di Lorenzo E, Combes V, Keister JE, Strub PT, Thomas AC, Franks PJS, Ohman MD, Furtado JC, Bracco A, Bograd SJ, Peterson WT, Schwing FB, Chiba S, Taguchi B, Hormazabal S, Parada C (2013a) Synthesis of Pacific Ocean climate and ecosystem dynamics. Oceanography 26(4):68–81. https://doi.org/10.5670/oceanog.2013.76

Di Lorenzo E, Mountain D, Batchelder HP, Bond N, Hofmann EE (2013b) Advances in marine ecosystem dynamics from US GLOBEC: the horizontal-advection bottom-up forcing paradigm. Oceanography 26(4):22–33. https://doi.org/10.5670/oceanog.2013.73

Frankignoul C, Hasselmann K (1977) Stochastic climate models, Part II Application to sea-surface temperature anomalies and thermocline variability. Tellus 29(4):289–305. https://doi.org/10.3402/tellusa.v29i4.11362

Frankignoul C, Czaja A, L'Heveder B (1998) Air-Sea feedback in the North Atlantic and surface boundary conditions for oceans models. J Clim 11:2310–2324. https://doi.org/10.1175/1520-0442(1998)011%3c2310:ASFITN%3e2.0.CO;2

Furtado JC, Di Lorenzo E, Schneider N, Bond NA (2011) North pacific decadal variability and climate change in the IPCC AR4 models. J Clim 24(12):3049–3067. https://doi.org/10.1175/2010jcli3584.1

Gillett N, Fyfe J (2013) Annular mode changes in the CMIP5 simulations. Geophys Res Lett 40:1189–1193. https://doi.org/10.1002/grl.50249

Joh Y, Di Lorenzo E (2017) Increasing coupling between NPGO and PDO leads to prolonged marine heat waves in the Northeast Pacific. Geophys Res Lett 44:11663–11671. https://doi.org/10.1002/2017GL075930

Kay JE, Deser C, Phillips A, Mai A, Hannay C, Strand G, Arblaster JM, Bates SC, Danabasoglu G, Edwards J, Holland M, Kushner P, Lamarque J, Lawrence D, Lindsay K, Middleton A, Munoz E, Neale R, Oleson K, Polvani L, Vertenstein M (2015) The Community Earth System Model (CESM) large ensemble project: a community resource for studying climate change in the presence of internal climate variability. Bull Am Meteorol Soc 96:1333–1349. https://doi.org/10.1175/BAMS-D-13-00255.1

Kelly KA et al (2010) Western boundary currents and frontal air-sea interaction: Gulf Stream and Kuroshio Extension. J Clim 23(21):5644–5667

Kouketsu S et al (2016) Mesoscale eddy effects on temporal variability of surface chlorophyll a in the Kuroshio Extension. J Oceanogr 72(3):439–451

Kwon Y, Alexander MA, Bond NA, Frankignoul C, Nakamura H, Qiu B, Thompson LA (2010) Role of the Gulf Stream and Kuroshio-Oyashio systems in large-scale atmosphere-ocean interaction: a review. J Clim 23:3249–3281. https://doi.org/10.1175/2010JCLI3343.1

Lorenz DJ (2014) Understanding midlatitude jet variability and change using rossby wave chromatography: poleward-shifted jets in response to external forcing. J Atmos Sci 71:2370–2389. https://doi.org/10.1175/JAS-D-13-0200.1

Mantua N, Hare S (2002) The pacific decadal oscillation. J Oceanogr 58:35–44. https://doi.org/10.1023/A:1015820616384

Minobe S (1999) Resonance in bidecadal and pentadecadal climate oscillations over the North Pacific: role in climate regime shift. Geophys Res Lett 26:855–858

Nakata K, Koyama S, Matsukawa Y (2011) Interannual variation in spring biomass and gut content composition of copepods in the Kuroshio current. Fish Oceanogr 10:329–341

Pierini S, Dijkstra HA (2009) Low-frequency variability of the Kuroshio extension. Nonlin Processes Geophys 16:665–675. https://doi.org/10.5194/npg-16-665-2009

Polovina EH, Kobayashi DR, Seki MP (2001) The transition zone chlorophyll front, a dynamic global feature defining migration and forage habitat for marine resources. Progress Oceanogr 49(1–4):469–483. https://doi.org/10.1016/S0079-6611(01)00036-2 (**ISSN 0079-6611**)

Polovina J, Howell E, Kobayashi D, Seki M (2015) The transition zone chlorophyll front updated: advances from a decade of research. Prog Oceanogr. https://doi.org/10.1016/j.pocean.2015.01.006

Qiu B (2002) The Kuroshio extension system: its large-scale variability and role in the midlatitude ocean-atmosphere interaction. J Oceanogr 58:57–75. https://doi.org/10.1023/A:1015824717293

Qiu B (2003) Kuroshio extension variability and forcing of the pacific decadal oscillations: responses and potential feedback. J Phys Oceanogr 33:2465–2482. https://doi.org/10.1175/2459.1

Qiu B, Chen S (2005) Variability of the Kuroshio extension jet, recirculation gyre, and mesoscale eddies on decadal time scales. J Phys Oceanogr 35:2090–2103. https://doi.org/10.1175/JPO2807.1

Qiu B et al (2007) Coupled decadal variability in the North Pacific: An observationally constrained idealized model. J Clim 20(14):3602–3620

Sasai Y, Sasaoka K, Sasaki H, Ishida A (2007) Seasonal and intraseasonal variability of chlorophyll-a in the North Pacific: model and satellite data. J Earth Simul 8:3–11

Sasaki YN, Schneider N (2011) Decadal shifts of the Kuroshio extension jet: application of thin-jet theory. J Phys Oceanogr 41(5):979–993. https://doi.org/10.1175/2011JPO4550.1

Sonnewald M, Wunsch C, Heimbach P (2018) Linear predictability: a sea surface height case study. J Climate 31:2599–2611. https://doi.org/10.1175/JCLI-D-17-0142.1

Storch H, Zwiers F (1999) Statistical analysis in climate research. Cambridge University Press, Cambridge. https://doi.org/10.1017/CBO9780511612336

Sydeman WJ, Santora JA, Thompson SA, Marinovic B, Di Lorenzo E (2013) Increasing variance in North Pacific climate relates to unprecedented ecosystem variability off California. Glob Change Biol 19(6):1662–1675. https://doi.org/10.1111/gcb.12165

Taguchi B, Xie S-P, Mitsudera H, Kubokawa A (2005) Response of the Kuroshio extension to Rossby waves associated with the 1970s climate regime shift in a high-resolution ocean model. J Clim. https://doi.org/10.1175/JCLI3449.1

Taguchi B, Xie S, Schneider N, Nonaka M, Sasaki H, Sasai Y (2007) Decadal variability of the Kuroshio extension: observations and an eddy-resolving model hindcast. J Climate 20:2357–2377. https://doi.org/10.1175/JCLI4142.1

Taguchi B, Qiu Bo, Nonaka M, Sasaki H, Xie S-P, Schneider N (2010) Decadal variability of the Kuroshio extension: mesoscale eddies and recirculations. Ocean Dyn 60:673–691. https://doi.org/10.1007/s10236-010-0295-1

TOPEX/Poseidonand ERS-1 and -2.J. Geophys Res 105: 19 477–19 498, https://doi.org/10.1029/2000JC900063

Vallis GK, Zurita-Gotor P, Cairns C, Kidston J (2015) Response of the large-scale structure of the atmosphere to global warming. Quart J R Meteorol Soc 141:1479–1501. https://doi.org/10.1002/qj.2456

Wu B, Lin X, Qiu B (2019) On the seasonal variability of the Oyashio extension fronts. Clim Dyn 53:7011–7025. https://doi.org/10.1007/s00382-019-04972-1

Yang Y, San Liang X (2018) On the seasonal eddy variability in the Kuroshio extension. J Phys Oceanogr 48:1675–1689. https://doi.org/10.1175/JPO-D-18-0058.1

Yang H, Lohmann G, Wei W, Dima M, Ionita M, Liu J (2016) Intensification and poleward shift of subtropical western boundary currents in a warming climate. J Geophys Res Oceans 121:4928–4945. https://doi.org/10.1002/2015JC011513

Yang Y, San Liang X, Qiu B, Chen S (2017) On the decadal variability of the eddy kinetic energy in the Kuroshio e xtension. J Phys Oceanogr 47:1169–1187. https://doi.org/10.1175/JPO-D-16-0201.1

Yatsu A, Chiba S, Yamanaka Y, Ito S-I, Shimizu Y, Kaeriyama M, Watanabe Y (2013) Climate forcing and the Kuroshio/Oyashio ecosystem. ICES J Mar Sci 70:922–933

Yi DL, Gan B, Wu L, Miller AJ (2018) The North Pacific Gyre oscillation and mechanisms of its decadal variability in CMIP5 Models. J Clim 31:2487–2509. https://doi.org/10.1175/JCLI-D-17-0344.1